Author's Accepted Manuscript

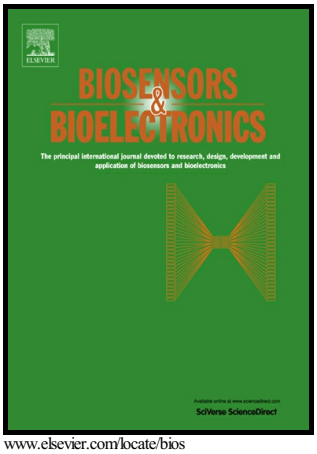

www.elsevier.com/locate/bios

Liquid Gated ZnO Nanorod FET Sensor for Ultrasensitive Detection of Hepatitis B Surface Antigen with Vertical Electrode Configuration

B. Chakraborty, S. Ghosh, N. Das, C. RoyChaudhuri

PII: S0956-5663(18)30703-6
DOI: https://doi.org/10.1016/j.bios.2018.09.019
Reference: BIOS10759

To appear in: *Biosensors and Bioelectronic*

Received date: 25 June 2018
Revised date: 2 September 2018
Accepted date: 4 September 2018

Cite this article as: B. Chakraborty, S. Ghosh, N. Das and C. RoyChaudhuri, Liquid Gated ZnO Nanorod FET Sensor for Ultrasensitive Detection of Hepatitis B Surface Antigen with Vertical Electrode Configuration, *Biosensors and Bioelectronic,* https://doi.org/10.1016/j.bios.2018.09.019

Liquid Gated ZnO Nanorod FET Sensor for Ultrasensitive Detection of Hepatitis B Surface Antigen with Vertical Electrode Configuration

B.Chakraborty[a], S.Ghosh[b], N.Das[a] and C.RoyChaudhuri[a,*]

[a]Department of Electronics and Telecommunication Engineering, Indian Institute of Engineering Science and Technology, Shibpur, West Bengal 711103, India

[b]Centre of Excellence for Green Energy and Sensor Systems, Indian Institute of Engineering Science and Technology (IIEST), Shibpur, Howrah, West Bengal 711103, India

[*]email: chirosreepram@yahoo.com

Abstract:

Detection of the Hepatitis-B surface antigen at the attomolar level is demonstrated using antibody functionalized liquid gated ZnO nanorods field effect transistor (FET) biosensor with vertical electrode configuration. The sensor is operated in heterodyne mode at high frequency to overcome the problem of Debye screening effect in physiological analyte. Enhanced penetration of the electric field lines through the nanorods enables significant improvement in the limit of detection and sensitivity compared to that of the conventional lateral electrode configuration. The combined effect of the probable change in the threshold voltage and the carrier mobility for vertical electrode configuration lead to a sensitivity of around 75% at 1 fM (which is an enhancement by 200%) and a detection limit of 20 aM with a dynamic range from 20 aM to 1 pM. The detection limit which is achieved with the proposed label free sensor in physiological analyte using antibodies is lowered by more than three orders of magnitude compared to the existing reports.

Keywords: **ZnO nanorods, liquid gated, FET sensor, ultrasensitive detection, vertical electrode**

1. Introduction:

Detection of viral infections like Hepatitis-B, Hepatitis-C, HIV and others are of utmost priority, not only for human health but also to ensure security against bioterrorism. Recurrent onset of Hep-B virus infection may lead to hepatocellular carcinoma and cirrhosis (Lee et al., 2012). Out of two billion Hep-B infected people, 350 million are chronically infected worldwide. Hep-B surface antigen (HBsAg) is a part of the Hep-B virus and is used as a biomarker for Hep-B infection (Bonino et al., 2010; Trépo et al., 1993). When the body gets exposed to Hep-B, HBsAg appears in the serum, which is the first serologic marker. One of the requisite for early

detection of HBsAg is ensuring an ultra low level of detection, such that even for trace quantities in presymptomatic condition, indication of antigen concentration is obtained.

HBsAg can be diagnosed using rapid diagnostic tests (RDT) in lateral flow or simple agglutination assay formats. Laboratory-based immunoassays for the detection of HBsAg include conventional methods like radioimmunoassay (RIA) and enzyme immunoassays (EIA), as well as latest technologies such as electrochemiluminescence immunoassays (ECLIA), chemiluminescent microparticle immunoassays (CMIA) and microparticle enzyme immunoassays (MEIA) (Amini et al., 2017). Virus detection techniques based on enzyme linked immunosorbent assay (ELISA) exist commercially which suffer from poor sensitivity, resulting in diagnosis at higher viral loads, typically of the order of nanomolars (Rutstein et al., 2014). This in turn enhances the treatment expenses. Thus, lowering the level of detection towards sub-femtomolar levels in physiological analyte by amplification of transduced signal is worthy investigating. One of the extensively used approaches for amplified signal transduction is the deployment of nanostructured materials in various configurations. Recent report on plasmonic gold nanoparticles (Hakimian et al., 2018) resulted in level of detection (LOD) in the aM range. An electronic adaptation of ELISA has been interfaced with indium oxide nanoribbons for virus detection down to sub-femtomolar regime (Aroonyadet et al., 2015). However, these technologies are not label free and require extensive biochemical processing. For point-of care diagnostic applications, label free nanostructured biosensors based on impedance, conductance and amperometric measurements have been extensively investigated. The widely fabricated nanostructures for this purpose include nanoribbons (Chen et al., 2013), nanowires (Li et al., 2015), ordered and random nanopores (Ghosh and Roychaudhuri, 2013), nanorods (Xue et al., 2015), nanotubes (Hidaka et al., 2016), nanogrids (Basu and Chaudhuri, 2016) and nanoparticles (Aydoğdu et al., 2013) on substrates like silicon and its oxide, carbon, graphene, indium oxide, zinc oxide, anodized alumina and various polymers. Amongst the different sensing mechanisms, FET based transconductance measurements on 1D silicon nanowires, carbon nanotubes and zinc oxide nanowires have been explored because of the intrinsic amplification effect (Lee et al., 2015; Marques et al., 2017). But their LODs are limited mostly in the pM range. This is attributed to the scarcity of available binding sites on the 1D nanoscale materials, especially in the fM or sub-fM range. We have reported FET based sensing of HBsAg in the aM range using graphene nanogrids (Basu and Chaudhuri, 2016) in buffer. However, in physiological samples,

the detection limits are supposed to be further deteriorated with high salt concentration due to Debye screening effect, whereby sensing in aM regime is indeed a challenge. This condition becomes severe for most of the antibody-antigen conjugates since their dimensions typically exceed the Debye screening length of 1 nm in physiological analytes like serum or urine. For HBsAg also, the condition will be severe since they are large molecules greater than 10 nm (Gilbert et al., 2005). In this aspect, we have previously reported nanostructured silicon oxide based impedance biosensor which shows an interesting peak frequency phenomenon, not affected by the Debye screening effect and the shift in the peak frequency can detect down to 0.1 fM HBsAg in serum (Chakraborty et al., 2017). However, their performance is largely affected by surface roughness of the pores and suffers from reliability issues (Das and RoyChaudhuri, 2015).

For FET biosensor, the problem of reduced Debye screening at high ionic strengths, has been addressed by two methods- applying a high frequency signal between drain and source which initiates breakdown of the electric double layer near FET channel surface and coating the FET channel surface with polyethylene glycol which enhances the effective screening length (Chu et al., 2017; Gao et al., 2015; Kulkarni and Zhong, 2012). In the former, fast switching of the applied bias leads to deeper penetration of the electric potential of target protein but its application in carbon nanotubes has resulted in only pM detection limit, the reasons for which have already been indicated. The latter method has been utilized in graphene and carbon nanotube FETs for detection of numerous biomolecules like prostate specific antigen, Zika virus, lead ions and brain natriuretic peptide (Afsahi et al., 2018; Gao et al., 2016; Lei et al., 2017; Wang et al., 2016). But the detection limits vary from nM to a few hundreds of fMs primarily because the thick functionalization layer results in weakened capacitive coupling leading to a decrease in transconductance. At this stage, it is evident, that development of FET based biosensors on a high surface area to volume ratio substrate with a high intrinsic transconductance is the need of the time. In this aspect, ZnO nanorod is a desirable material compared to graphene in terms of sensing application due to its high on-off ratio (Ahn et al., 2018). Additionally ZnO nanorods lead to enhancement of surface area to volume ratio and have been experimented for protein, virus and enzyme detection using optical, amperometric, impedance and transconductance principles (Ahmad et al., 2017a, 2017b, 2017c, 2013, 2014, 2015; Ahn et al., 2018; Dang et al., 2015; Fathollahzadeh et al., 2018; Han et al., 2016; Ibupoto et al., 2011;

Kumar et al., 2016; Zong et al., 2017). The detection limit obtained for virus is around few femtomolars in buffer (Han et al., 2016). ZnO nanorod integrated microfluidic biosensor has been reported (Yu et al., 2017) as a sensitive immunofluorescence platform for the detection of avian influenza virus (AIV). The high sensitivity has been attributed to the combined effect of faster carrier diffusion process of the biomolecules within the nanorod structures and enhanced capture of the surface probes. But, virus detection in physiological analyte using label free FET based ZnO nanorod structure has not yet been explored. The fM detection limit of virus in ZnO nanorod FETs in buffer can be extended to physiological analyte in the aM regime by adopting high frequency heterodyne mode of sensing and incorporating some signal amplification strategies. Here, we improve the electrical contact configurations for signal enhancement, which also does not impose any additional consumable burden. Presently, all the existing drain-source contacts are fabricated laterally below the ZnO seed layer and the biomolecules on the surface of the ZnO nanorods mostly affect the conduction of the seed layer indirectly. Conduction through ZnO nanorods is limited by the presence of available interconnections. On the contrary, if the contacts are fabricated vertically, one on the ZnO nanorod surface and the other at the bottom, there will be enhanced conduction through the nanorods and the direct impact of the surface potential alteration within the nanorods is expected to result in additional current change.

In this paper, electrical sensing of HBsAg as a target protein down to aM range in serum has been demonstrated on liquid gated ZnO nanorods. Firstly, implementing the high frequency heterodyne signal between the drain source contacts fabricated below the seed layer enable detection of HBsAg down to 1 fM in serum. But with the vertical drain-source contact configuration, the detection limit has been lowered to 20 aM through a sensitivity enhancement of more than 200%.

2. Materials and Methods:

2.1 Fabrication of ZnO Nanorod Based FET

For the fabrication of ZnO nanorods FET biosensor, low cost glass substrate has been used. ZnO nanorods based FET has been fabricated with two drain-source electrode configurations- lateral and vertical as depicted in Figure 1(a) and 1(b) respectively. For the former, on one side of the glass substrate, contacts have been fabricated by photolithography. Positive photoresist S1813 has been spin coated on the glass surface at 2500 rpm for 30 seconds and further it has

been dried at 100ºC on a hot plate for the evaporation of the solvent present in the resist. Then, the sample has been exposed under UV radiation by a mask aligner (MA6/BA6, make by Karl SUSS, Germany). Finally, after exposure under UV, the electrode pattern on the sample has been developed by developer MF 319. Post baking has been performed after developing the samples at 120ºC. After developing, a layer of Au(50nm)/Cr(100nm) has been deposited on lithographically defined area by thermal evaporation and the electrode patterns have been formed after lift-off process. The interdigited source-drain electrodes have been designed to have 10 μm spacing between each pair and width of the electrodes has been fixed at 2 mm. This is followed by the growth of ZnO seed layer has then been grown using sol-gel technique. For this purpose, 50mM zinc nitrate hexahydrate [$Zn(NO_3)_2$,$6H_2O$] has been mixed with 100ml DI water for the preparation of ZnO precursor solution. The solution bath has been set on a magnetic stirrer and heat has been provided. As soon as the bath temperature increases to 60°C, 4ml Ammonium Hydroxide [NH_4OH] solution has been added, followed by stirring for 30 minutes. After that, for 24 hours the solution bath has been kept undisturbed. ZnO film, obtained from the ZnO precursor solution, has been spin-coated on glass surface (Li et al., 2014). Subsequently, ZnO grown glass sample has been put on a hotplate for evaporation of the remaining solvent. In the second step, ZnO nanorods have been grown on the seeded area following previously reported procedure (Paul et al., 2014). 50 mM Zinc Nitrate Hexahydrate [$Zn(NO_3)_2$,$6H_2O$] has been mixed in 50ml DI water and stirred for 10 min. 50 mM Hexamethylenetetramine (HMTA: $C_6H_{12}N_4$) has been mixed with 50 ml DI water and this has also been stirred for 10 min. Then both the solution baths have been mixed together and stirred at 260 rpm. The ZnO seeded glass substrate has been suspended into the solution bath for 2 hours. Following this, the glass substrate has been taken out from the solution bath and washed with DI water. To achieve better crystallization, the ZnO nanorods have been annealed at 350°C for 5 min using rapid thermal annealing method.

For vertical electrode configuration, the source contact with interdigited pattern connected with a single bond pad, has been developed on one side of the glass substrate prior to ZnO seed layer growth. After that, ZnO seed layer and ZnO nanorods have been grown. Then, the interdigited pattern of the drain contact with a bond pad has been fabricated on top of the ZnO nanorods. Au(50nm)/Cr(100nm) source and drain interdigited electrodes have been fabricated following the same photolithography process as that for lateral electrode.

To confirm that the sensors with the vertical electrode configuration have been fabricated successfully, electrical resistance has been initially measured between the top and bottom drain and source contacts. This test reveals whether there is any unwanted short circuited path between the two. The presence of a short circuit will indicate faulty fabrication. We have not observed the presence of any short circuited path and the typical value of the drain to source resistance (R_{ds}) at zero gate to source voltage (V_{gs}) has been found out to be higher than 100 kΩ. Further, we have confirmed the ZnO deposition through UV absorption spectroscopy and photoluminescence characterization. These results have been discussed in Section 3.1.

2.2 Functionalization of ZnO

For proper antibody immobilization, silanization process has been followed by crosslinker attachment. The silane solution has been prepared using 0.4 ml MTS (3-mercaptopropyltrimethoxysilane) and 9.258 ml ethanol with 0.341ml DI water and pipetted on ZnO sensor surface. The sensor has been sealed and left in nitrogen environment for 24 hours. Following this, the excess silane solution has been discarded and the sample has been washed in ethanol. Then ultra-sonication has been carried out in ethanol for 5 minutes, followed by a drying session in N_2 environment. For the crosslinker attachment step, 2mM GMBS solution has been pipetted onto the ZnO surface and left to interact for 24 hours. The sample has then been ultrasonicated in ethanol for about 5 minutes. The activated ZnO surface is now suitable for the covalent attachment of antibodies. All surface modification steps have been performed at room temperature, following previously reported procedure(Corso et al., 2008). For the estimation of the antibody binding intensity, optical density (O.D.) measurements have been carried out using horse radish peroxidise (HRP) conjugated Human IgG (HRP-HIgG). For colour test, a standard colouring reagent solution has been prepared, as reported by Dev Das and colleagues (Das et al., 2010). Anti-Hep-B monoclonal antibodies have then been immobilized on the ZnO nanorod based sensor surface. A well like structure has been fabricated using polydimethylsiloxane (PDMS) sheets. It has been bonded with the biosensor surface using plasma treatment to avoid fluctuations occurring from positioning of the solution droplet. This method ensures repeatability of measurements. Polyethylene tubing has been attached as the inlet and outlet of the PDMS wells through which virus and buffer solutions have been drawn using a syringe pump. Firstly, buffer solution has been pumped through the inlet at an optimized flow rate of 130µl/min and

after it has stabilized, the pump has been switched off and the electrical reading has been recorded. Under this situation, the inlet and outlet tubings are both filled with buffer. Then 20µl of analyte, i.e. serum has been injected at the inlet using the same pump at the rate of 2.5µl/min. The analyte now diffuses towards the sensor surface and the electrical readings have been recorded to identify the presence of specific molecules.

2.3 Antigen Solution Preparation

HBsAg has been taken as the target molecule which has been purchased from US Biological, USA (1 mg/ml). For the purpose of measurement, serial dilutions of HBsAg solution has been performed in PBS with pH 7.2 and 100 mM ionic strength to produce concentrations ranging from 0.01fM to 1 pM of Hep-B. For measurements in physiological analyte, HBsAg has been spiked in blood serum. The blood samples collected from a microbiological laboratory have been kept for some time at room temperature to separate the serum. The specificity of the fabricated FET biosensor has been tested with CEA, HBeAg, IgG, PSA and BNP molecules by spiking separately 1nM concentration of each of them in serum.

2.4 Electrical Measurement

Each sensor chip has been interfaced with the PC through a sensor holder set up. In the setup, the bond pads of the sensors have been placed below the probes of the sensor holder. The probes of the sensor holder which are in contact with the drain and source electrodes are spring loaded and adjustment screws have been provided to align them with the bond pads. The gate electrode has been inserted through a small hole in the setup and soldered to a metal connector. The gate electrode has been connected to a dc power supply (Keysight technologies). A high frequency signal of 20 mV amplitude in the range of 200 kHz to 1000 kHz has been applied through a signal generator (Agilent 33521A) at the drain electrode. It has been modulated by a reference signal of 1.43 kHz using a lock-in amplifier (Stanford Research, SR 830) and fed to the ZnO FET at the source. The root mean square value of the mixing current through the drain terminal has been detected at the modulated frequency, both before and after application of the analyte. All the measurements have been noted using five samples and their means along with the standard deviations have been represented.

2.5 Implementation of Different Characterization Techniques

To characterize the surface morphology of the ZnO nanorods, field emission scanning electron microscopy (*ZEISS EVO-MA 10*) has been used. X-Ray diffraction (XRD) characterization technique (*RigakuMiniFlex X-ray diffractometer*) has been employed to examine the crystal structure of the ZnO nanorods. Surface profilometry (*Dektak ST3*) has also been carried out to estimate the thickness of the ZnO seed layer. To observe the fabricated interdigited electrodes on ZnO nanorod surface, an optical microscope (*OPTIKA B-600*) has been used. For the estimation of antibody binding density, optical density (O.D.) measurements have been performed with a UV-VIS spectrophotometer (*Perkin Elmer Lamda 25*). The spectrophotometer has also been used to measure the absorption spectrum of ZnO nanorods. Photoluminiscence measurement has been carried out on the ZnO grown glass sample using Raman and MicroPL System (*LabRAM HR Evolution*).

3. Results and Discussion:

3.1 Structural and Optical Characterization

The schematic illustration of the FET sensor with the different electrode configurations are shown in Figure 1(a) and 1(b). Overall picture of the FET sensor has been displayed in Figure 1(c). XRD pattern of the ZnO nanorods (post annealing) has been represented in Figure S1(a). ZnO nanorods grown on glass surface exhibit diffraction peak in [0002] plane at $2\theta \approx 34.4°$. The rapidly grown [0002] diffraction peak denotes hexagonal growth of ZnO crystal with its c-axis perpendicular to the glass substrate. Clear sharpness of the XRD diffraction peak justifies the crystallinity of the grown ZnO nanorods. Surface profilometry result provides the information on surface roughness. Thickness of the ZnO seed layer which has been grown prior to nanorod growth, has been found out to be around 45nm (Figure S1(b)) from the profilometry result. FESEM micrograph of the ZnO seed layer has been shown in Figure 2(a). Seed layer film continuity can be confirmed from this micrograph. Average grain size has been observed to be around 60nm from FESEM result.

Surface morphological study has been carried out using high resolution FESEM set up, with an operating voltage of 10 kV. The top-view FESEM micrograph of the grown ZnO nanorod sample just beside the electrodes has been shown in Figure 2(b). The uneven metal edges may be attributed to the non-uniformity in the lift-off process owing to the roughness of the ZnO nanorod surface. Highly densed and vertically aligned ZnO nanorod arrays can be noticed in the

FESEM micrograph of Figure 2(c). FESEM image of the sensor surface after antibody attachment is shown in Figure 2(d). The length of the grown ZnO nanorods is around 1.54 μm and diameter is estimated to be 228 nm. Figure S2 shows optical microscope image of the fabricated interdigited electrodes on ZnO nanorod surface. Absorption spectrum of ZnO nanorods, grown glass samples has been shown in Figure S3(a) using UV VIS spectrophotometer. From that absorption spectrum, bandgap of the grown ZnO has been calculated (Figure S3(b)) to be 3.21 eV. Supplementary figure (Figure S4) represents photoluminiscence spectrum of the ZnO nanorods. Immobilized antibody density has been obtained for both the electrode configurations, from optical density measurements technique using UV VIS spectrophotometer, following the methodology reported previously (Das et al., 2010). The absorbance spectra obtained from the antibody coated sensor surface for lateral and vertical electrode configurations, have been represented in Figure S5. The existence of peak absorbance at around 280 nm for both the spectra confirms the presence of antibodies. Similar peak intensity for both the cases reveals that the available surface area for antibody binding is almost close. From the calibration data of the instrument, the number of immobilized antibody molecules on the sensor surface is found out to be in the order of 10^{10}. Considering the approximate molecular weight of the antibodies to be 24kDa (Cerino et al., 2015), the approximate mass of the attached antibody has been found out to be 0.398ng.

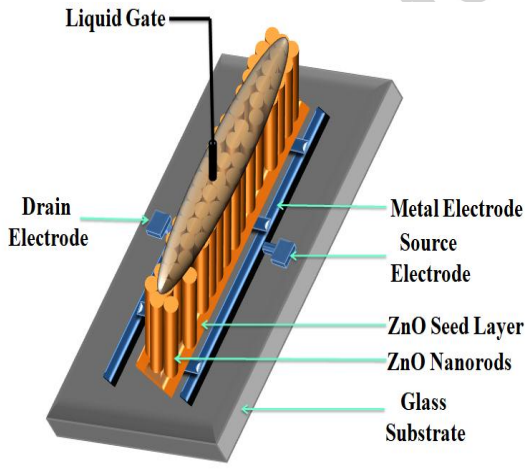

Figure 1.(a)

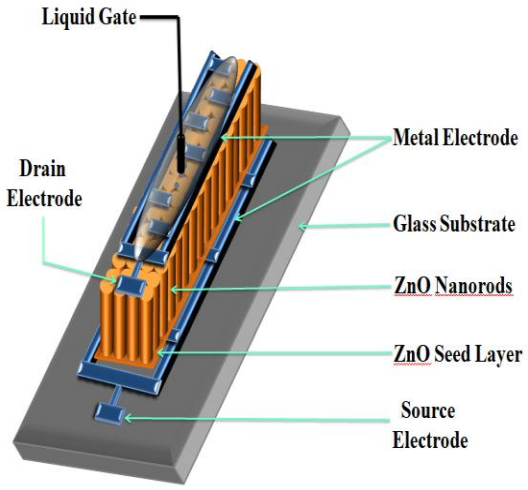

Figure 1.(b)

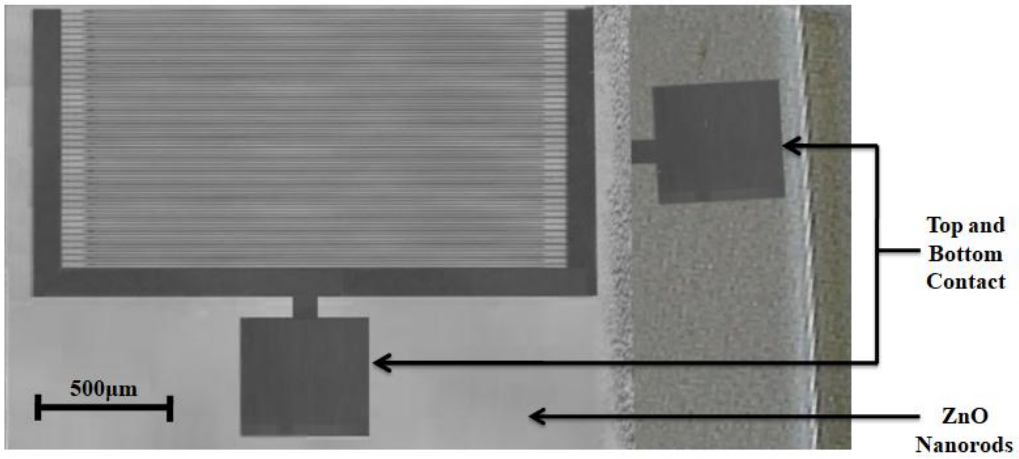

Figure 1.(c)

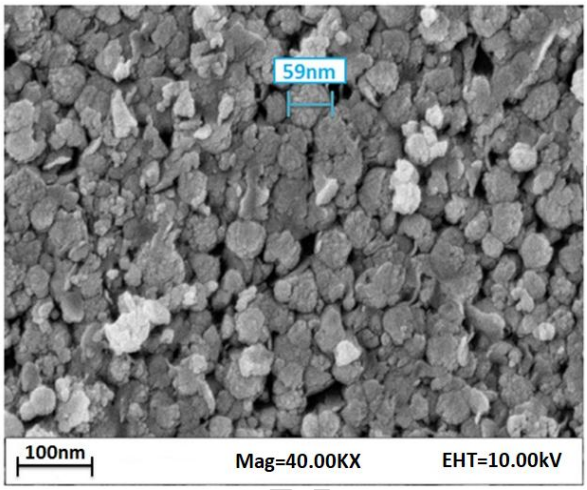

Figure 2.(a)

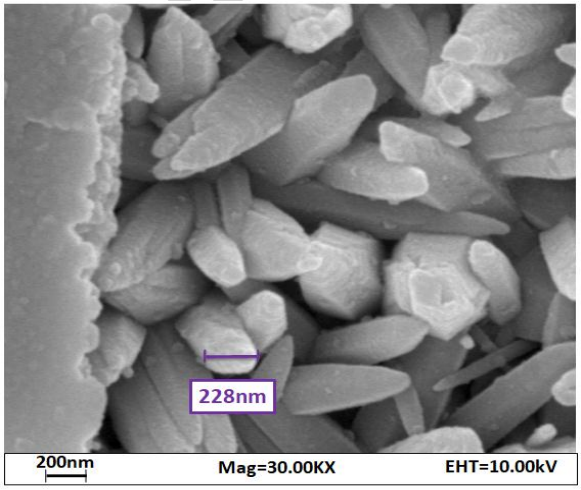

Figure 2.(b)

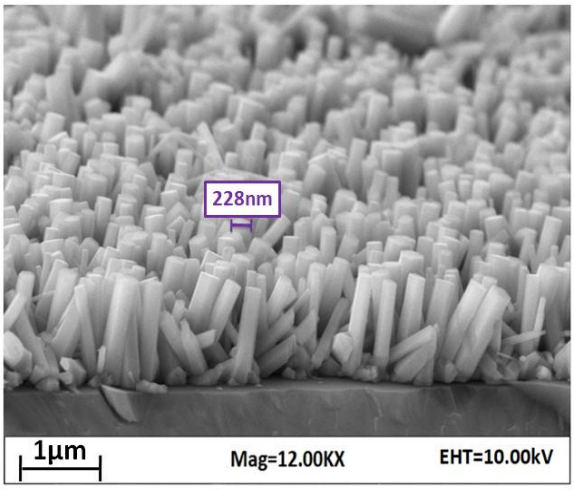

Figure 2.(c)

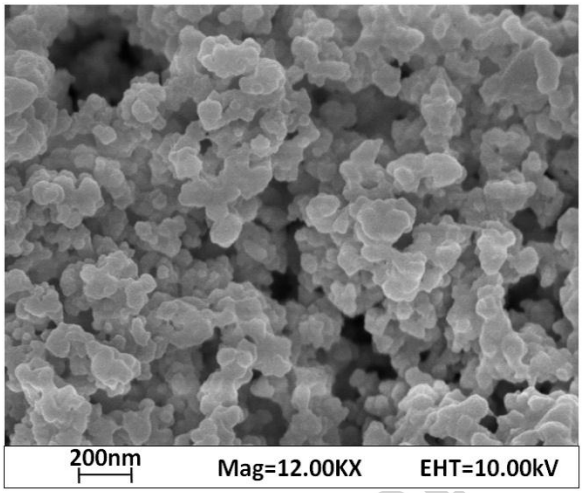

Figure 2.(d)

3.2 FET Studies of ZnO Nanorods

The variation of drain current (I_d) with gate to source voltage (V_{gs}) before and after antibody functionalization in presence of 100 mM buffer and for different frequencies at V_{ds} of 5V has been plotted in Figure 3(a) and 3(b). The increase in I_d with increasing V_{gs} indicates the n-type doping of the ZnO nanorods. It is observed that the current increases by more than two orders of magnitude for a change in V_{gs} from 0 to 5V which is indicative of high transconductance. Further, the current decreases after antibody functionalization in lateral electrode configuration and increases in vertical electrode configuration. This may be attributed to the positive charges of the antibody molecules at pH 7.2 (Choi et al., 2014), which causes a modulation of the applied gate voltage, resulting in additional accumulation of electrons within the nanorods. In lateral electrode configuration, this accumulation leads to a corresponding depletion within the seed layer resulting in a decrease of I_d. On the contrary, in vertical electrode configuration, the resistance of the nanorods dominate that of the seed layer's since their length is significantly higher than the thickness of the latter. Thus, the accumulation of electrons within the nanorods results in increase of I_d after antibody functionalization. Further, it is also interesting to note that the magnitude of I_d is appreciably more in the vertical electrode configuration compared to the lateral electrode one. This may be ascribed to the fact that the electric field lines between the drain-source electrodes penetrate larger sections of the nanorods, whereby increased number of carriers participate in conduction.

To further strengthen the explanation, the electric field line distributions for both the configurations of electrodes have been simulated using finite element method of COMSOL Multiphysics 4.3b. Semiconductor module has been selected to define ZnO. Figure 3(c) and 3(d) represent ideal and practical nanorod structures respectively with perpendicular and inclined orientations. Figure 3(e) indicates the vertical electrode configuration on the ideal nanorod structure. An electric potential has been applied in drain terminal and source terminal has been kept grounded. All other boundaries have been indicated as insulation. Due to strict memory and runtime limits, the spacing between the electrodes has been shown to be of similar order as that of the spacing between the nanorods. However, in practical device, the distance between the contacts is 10 times more than that of the length of the nanorods. But even the simplified electrode configuration is expected to reveal the difference in the electric field line distribution. A high density mesh has been considered within the constraint of executing the simulation in reasonable time. The larger structures have been described with relatively fewer vertices, whereas much more vertices have been required to faithfully describe the thin layers. Computational domain has assumed a room temperature with the parameters, T = 300 K, ε_r= 8.3, band gap E_g= 3.21eV,effective density of states of valence band and conduction band N_V= 1.13*10^{13} /m^3 and N_C= 2.72*10^{12} /m^3, electron mobility μ_n=0.025 m^2/Vs and conductivity σ=34 S/m(Liu et al., 2015). In the steady state continuum regime, the electric field distribution is guided by Maxwell-Boltzman theory (equation 1) which describes the potential distribution within nanorods and seed layer.

$$\nabla.(\varepsilon \nabla V) = -q(p - n - C) \quad (1)$$

where C=N_D-N_A+ρ_p-ρ_n, q is the electron charge, ε is the permittivity, p and n are the hole and electron concentrations respectively and C is the concentration of additional, typically fixed, charges. These fixed charges can originate from charged impurities of donor (N_D) and acceptor (N_A) and from trapped holes (ρ_p) and electrons (ρ_n).

To solve the model the semiconductor interface uses these definitions in combination with current continuity equations (equation 2).

$$\frac{1}{q}\nabla.J_n = -U_n \quad ; \frac{1}{q}\nabla.J_p = -U_p \quad (2)$$

where U_n=Σ$R_{n,i}$-Σ$G_{n,i}$ is the net electron recombination rate from all generation ($G_{n,i}$) and recombination mechanisms ($R_{n,i}$). Similarly U_p is the net hole recombination rate from all generation ($G_{p,i}$) and recombination mechanisms ($R_{p,i}$).

It is evident from Figure 3(c) and 3(d) that most of the field lines concentrate within the seed layer. For interconnected nanorods, the field lines penetrate them upto the common junction, whereas for vertical electrode configuration, most of the field lines are concentrated within the nanorods. Thus, for lateral electrode configuration, conduction of electrons take place mostly through seed layer, whereas for vertical electrode configuration electron conduction occurs through both the nanorods as well as seed layer which is expected to lead to different biomolecule detection sensitivity. This electrical conduction mechanism can be represented using equivalent resistance model depicted in Figure 3(f) and 3(g) which indicates that for vertical electrode configuration, the equivalent resistance of nanorods appear in series to that of the seed layer. The thickness of the seed layer being significantly smaller than that of the nanorods, the effect of the nanorods dominates. For lateral electrode configuration, the resistances appear in shunt with each other and for ideal nanorod structure, the seed layer resistance dominates. Additionally, it is to be noted from Figure 3(a) and 3(b) that, the fractional change in current ($\Delta I_d/I_d$) decreases after antibody immobilization with decreasing frequency. This may be attributed to the breakdown of the electric-double-layer (EDL) near the surface of the FET nanorods at high frequencies, due to fast switching of the direction of the applied bias, leading to deeper penetration of the electric potential within the antibodies (Kulkarni and Zhong, 2012). Supplementary figure (Figure S6(a) and S6(b)) represents the variation of I_d with V_{ds} for V_{gs} of 5V. The current saturates at a voltage of around 1V.

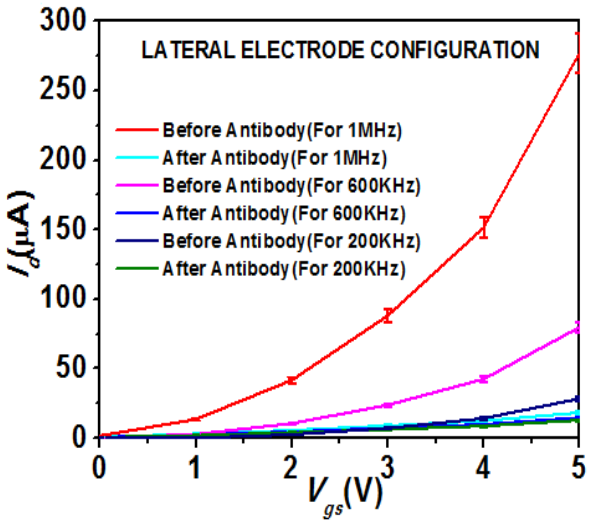

Figure 3.(a)

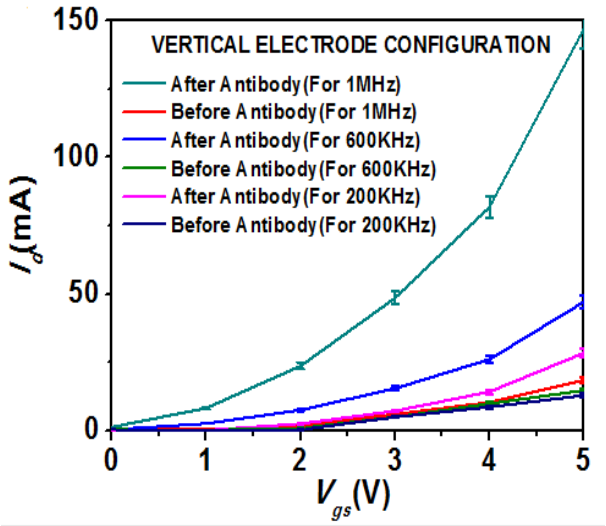

Figure 3.(b)

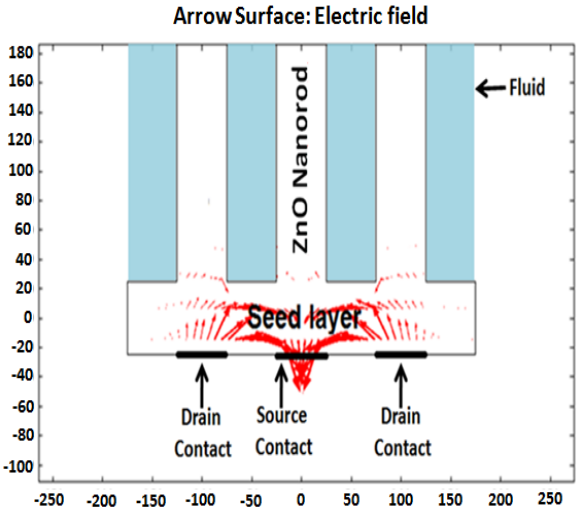

Figure 3.(c)

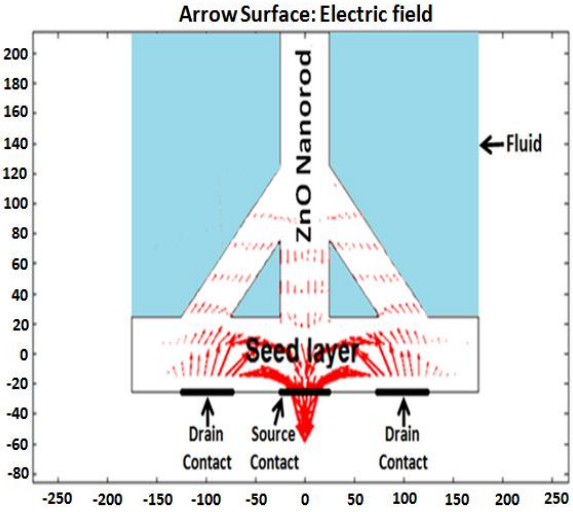

Figure 3.(d)

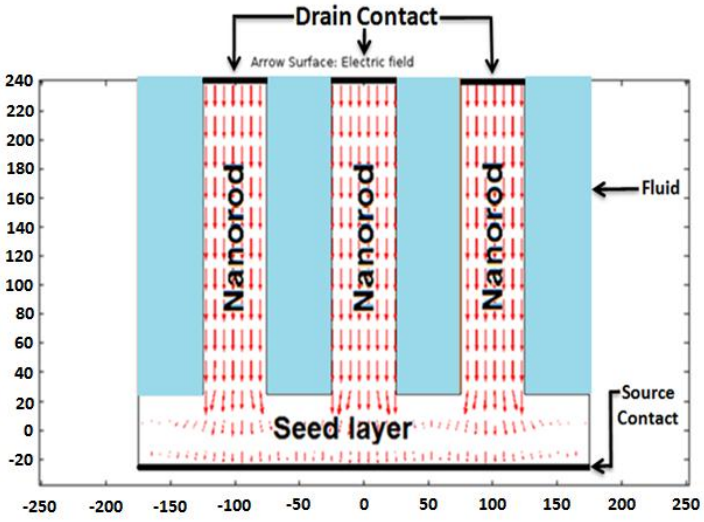

Figure 3.(e)

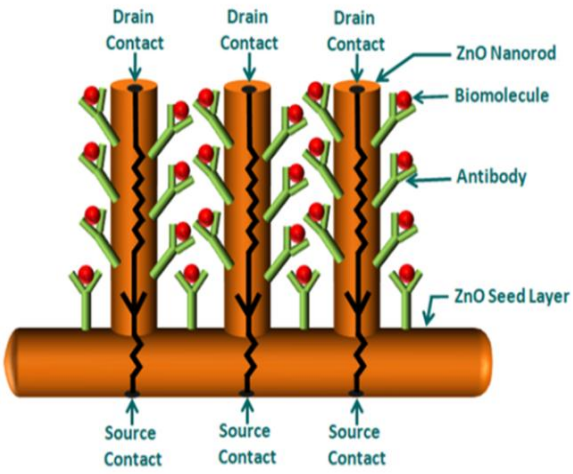

Figure 3.(f)

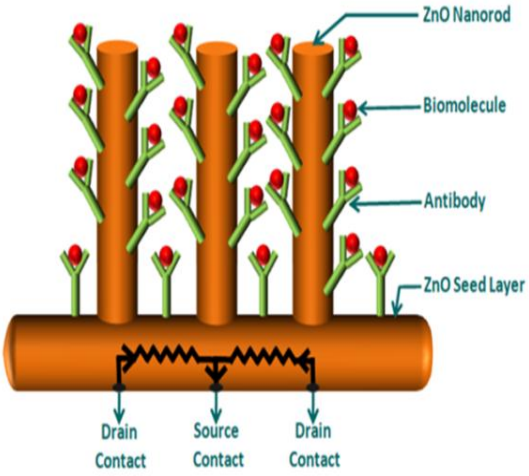

Figure 3.(g)

3.3 ZnO Nanorod Based Hep-B Surface Antigen Sensing

The variation of I_d with V_{gs} after HBsAg capture has been plotted in Figure 4(a) and 4(b) for different antigen concentration. It has been noticed from the plots that the drain current increases after HBsAg capture for lateral electrode configuration and decreases for vertical electrode configuration, compared to its value after antibody functionalization. This may be ascribed to the negative charge of HBsAg, which results in depletion of electrons within the nanorods which in turn results in accumulation within the seed layer. Thus, for lateral electrode configuration, as current conduction mostly takes place through the seed layer, I_d increases. For vertical electrode

configuration, current flows through both the nanorods and the seed layer in series. As the thickness of the seed layer is significantly smaller than that of the nanorods, the resistance of the nanorods dominates. Thus, the depletion of electrons within the nanorods after HBsAg capture leads to decrease in I_d in vertical electrode configuration. Figure S7(a) and S7(b) show I_d variation with V_{gs} at different frequencies after 1fM antigen capture. It is observed that the sensitivity is the maximum for 1 MHz frequency due to reasons stated in Section 2.2. I_d variation with antigen concentration at different frequencies has been plotted in Figure S8(a) and S8(b) for V_{gs} of 4 V. It is observed that the change in I_d is more in vertical electrode configuration that lateral electrode which is expected to increase the sensitivity in former. Variation of sensitivity with antigen concentration, has been plotted in Figure 4(c) and 4(d) for different frequencies at V_{gs} of 4 V. For direct comparison between the lateral and vertical electrode configuration, Figure 4(e) shows the sensitivity variation with antigen concentration at 1MHz frequency for both the electrode configurations. It is observed from these graphs that the relative standard deviations in sensitivity are within 5% for both the electrode configurations. Further, it indicates that in lateral electrode configuration, the detection limit cannot go beyond 1fM since below this concentration, the sensitivity falls to around 5% which cannot be reliably measured. On the other hand, in vertical electrode configuration, the detection limit can be reduced by two orders of magnitude to 0.02 fM with a sensitivity of around 20%. This is further justified from the observation that at 1fM antigen concentration, for vertical electrode configuration, sensitivity increases by more than 200% compared to that of lateral electrode configuration. This phenomenon may be explained using the resistance model represented in Figure 3(f) and 3(g) which indicates that for vertical electrode configuration, the equivalent resistance of nanorods appear in series to that of the seed layer. As the thickness of the seed layer is notably smaller than that of the nanorods, the effect of the nanorods dominates. But for lateral electrode configuration, the resistances appear in shunt with each other and for ideal nanorod structure, the seed layer resistance dominates. Biomolecules on the surface of the ZnO nanorods mostly affect the threshold voltage of the seed layer whereas within the nanorods, the surface potential gets altered additionally (as observed from the COMSOL simulation in Figure S9), which also affects the carrier mobility along with the threshold voltage (Nam et al., 2015). This effect may be responsible for the enhanced sensitivity.

The specificity of the highly sensitive ZnO biosensor with vertical electrode configuration has been tested at 1MHz frequency and V_{gs} of 4V using CEA, HBeAg, IgG, PSA and BNP molecules in serum by measuring the drain current sensitivity. It has been observed from Figure 4(f) that even at such high concentrations, the sensitivity is within 10% which determines the specificity of the sensor.

From the practical implementation point of view, lowering the detection limit of HBsAg in human serum will help in initiating early medical treatment which can eventually reduce the treatment cost and mortality. The comparison of the fabricated biosensor in analytical performance with previously reported sensors for HBsAg detection has been represented in Table 1. It is observed that the proposed ZnO sensor with vertical electrode configuration lowers the detection limit by more than two orders of magnitude compared to the most sensitive reports.

To validate the fabricated biosensing system, the results from the proposed sensor have been compared with the chemiluminescent immunoassay method (Architect HBsAg QT, Abbott Laboratories, US) which is widely used in clinical practice. Ten test solutions of HBsAg in blood serum have been prepared, keeping in mind the detection limit of the commercial system. As the detection limit of the proposed sensor is lower, the solutions have been further diluted by a known factor, before testing with the sensor. The measurements obtained from the commercial system have been divided by the known dilution factor and correlated with that from the sensor. It has been observed from Table 2 that the results from the sensor quantitatively agree with that of the reference within 7%.

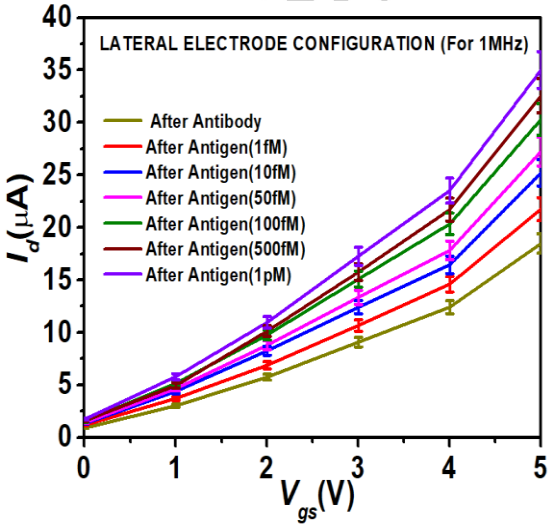

Figure 4.(a)

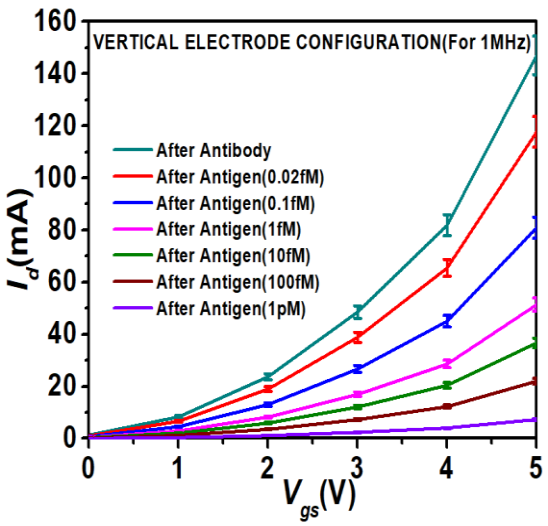

Figure 4.(b)

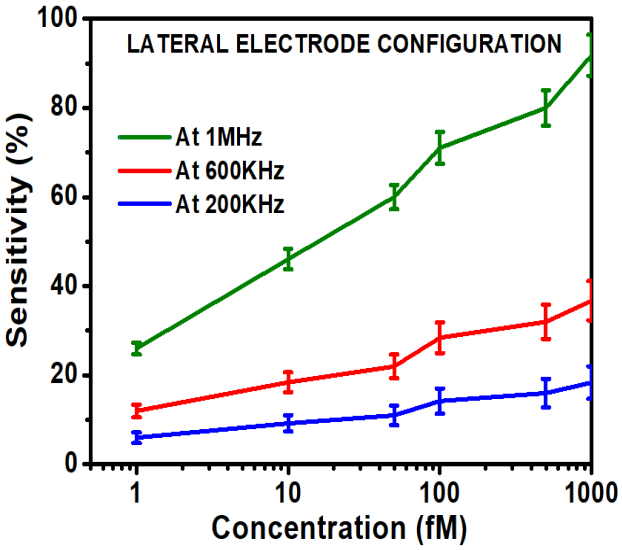

Figure 4.(c)

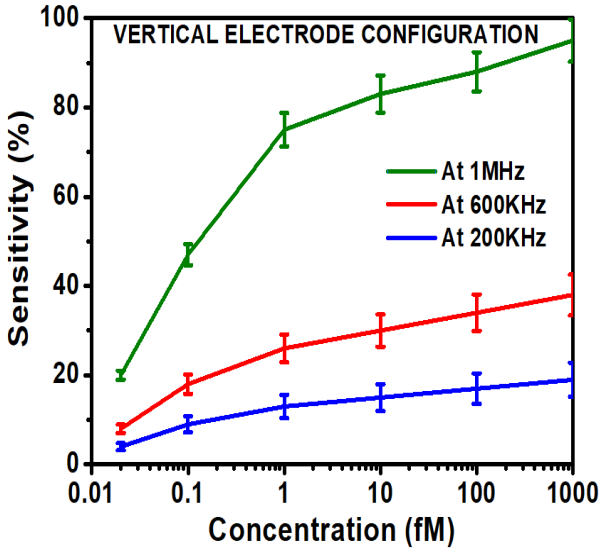

Figure 4.(d)

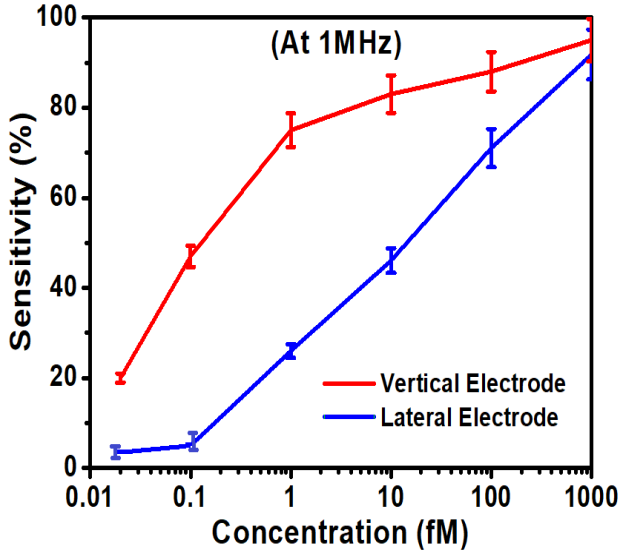

Figure 4.(e)

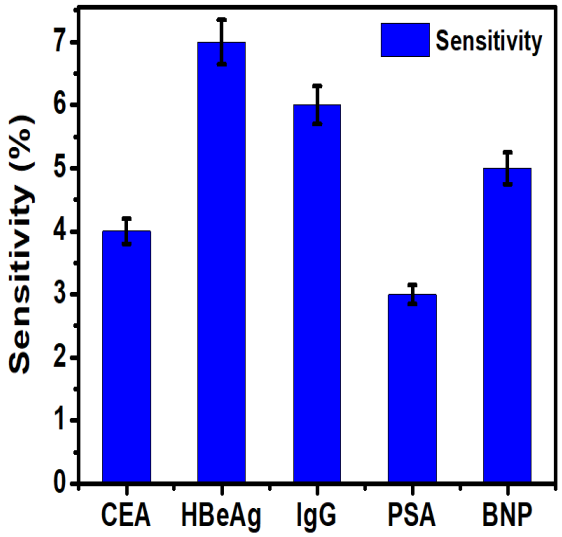

Figure 4.(f)

References	Method of detection	LOD	Sensitivity
(Shakoori et al., 2014)	FET sensor, label free	1 fM	58.2% @ LOD
(Shariati, 2018)	Electrochemical, label free	1 nM	55% @ LOD
(Xiang et al.,	Optical sensor, label free	40 fM (in PBS)	4 particulate matter (pm) (in PBS) @

2018)		400 fM (in serum)	LOD 60 pm(in serum)@ LOD
(Ahangar and Mehrgardi, 2017)	Electrochemical, label free	3.2 μM	ΔI = 600 nA @ LOD
(Eksin and Erdem, 2016)	Electrochemical, not label free	2 pM	ΔI = 0.2μA@ LOD
(Das et al., 2015)	Impedance sensor, label free	1 fM(in buffer) 1 fM (in serum)	20% (in buffer)@ LOD 25% (in serum)@ LOD
(Basu et al., 2018)	FET sensor, label free	1 fM(in buffer) 1 fM (in serum)	52% (in buffer) 36% (in serum)
This Paper	ZnO FET sensor with vertical electrode, label free	20aM (in serum)	75% @ 1 fM and 20% at LOD

Table 1.

Test Solutions of HBsAg	**Results**	
	Using ZnO FET Biosensor with Vertical Electrode Configuration	**Using chemiluminescent immunoassay method**
1pM	1.072pM	1.03pM
0.5pM	0.549pM	0.523pM
0.1pM	0.109pM	0.104pM
0.02pM	0.022pM	0.021pM
0.05pM	0.055pM	0.053pM

0.01pM	0.012pM	0.011pM
1fM	1.145fM	1.071fM
0.05fM	0.057M	0.054fM
5fM	5.618fM	5.251fM
0.02fM	0.023fM	0.021fM

Table 2.

3.4 Dynamic Response and Repeatability Study of ZnO Nanorod Sensor

The time dependent variation of I_d for two different concentrations of HBsAg spiked in serum has been plotted in Figure S10 for vertical electrode configuration. It has been observed that the current decreases exponentially which is an indication that the binding kinetics follow a Langmuir isotherm. Further, the time taken to reach the steady state is approximately 1000 seconds for both the concentrations which imply that the product of analyte concentration(c) and association rate constant (k_{on}) is negligible compared to dissociation rate constant (k_{off}). Thus the sensors are capable of real time operation.

For repeatability studies, the drift of the baseline current and the sensitivity of the ZnO nanorod sensor in vertical electrode configuration have been monitored for three months after antibody immobilization. During this time, the samples have been stored at -20^0C to preserve the functionality of the antibodies. It has been observed that the baseline current drifts by a maximum of 5% and the sensitivity for 0.02 fM HBsAg fluctuates within 3%.

4. Conclusion:

To summarize, in this paper, it has been demonstrated that FETs with ZnO nanorod array, operated in heterodyne mode at high frequency and immobilized with antibody probes can be applied for label free ultra-sensitive detection of HBsAg with a detection limit as low as 20 aM in physiological analyte using vertical electrode configuration. This has been possible due to a 200% sensitivity amplification compared to lateral electrode configuration, attributed to the

enhanced penetration of the electric field lines within the nanorods in the vertical electrode configuration which resulted in a combined change of carrier mobility and threshold voltage within the nanorod FETs. The detection limit achieved with the proposed label free sensor in physiological analyte using antibodies is lowered by two orders of magnitude compared to the most sensitive reports on HBsAg.It may be anticipated that this sensors can be extended for ultrasensitive detection of protein biomarkers of many diseases, including several types of cancers. However, fabrication of sensor array for multiple analyte detection with vertical electrode configuration is challenging and requires further investigation in the processing steps.

Acknowledgement:

This research has been supported by Visvesvaraya PhD Scheme and Visvesvaraya Young Faculty Research Award funded by the Ministry of Electronics & Information Technology, Government of India. One of the authors, Mr. N. Das would like to acknowledge UGC-RGNF for providing his fellowship.

References:

Afsahi, S., Lerner, M.B., Goldstein, J.M., Lee, J., Tang, X., Bagarozzi, D.A., Pan, D., Locascio, L., Walker, A., Barron, F., Goldsmith, B.R., 2018. Biosens. Bioelectron. 100, 85–88.

Ahangar, L.E., Mehrgardi, M.A., 2017. Bioelectrochemistry 117, 83–88.

Ahmad, R., Ahn, M.S., Hahn, Y.B., 2017a. J. Colloid Interface Sci. 498, 292–297.

Ahmad, R., Tripathy, N., Ahn, M.S., Bhat, K.S., Mahmoudi, T., Wang, Y., Yoo, J.Y., Kwon, D.W., Yang, H.Y., Hahn, Y.B., 2017b. Sci. Rep. 7, 1–10.

Ahmad, R., Tripathy, N., Ahn, M.S., Hahn, Y.B., 2017c. Sci. Rep. 7.

Ahmad, R., Tripathy, N., Hahn, Y.B., 2013. Biosens. Bioelectron. 45, 281–286.

Ahmad, R., Tripathy, N., Jung, D.U.J., Hahn, Y.B., 2014. Chem. Commun. 50, 1890.

Ahmad, R., Tripathy, N., Park, J.H., Hahn, Y.B., 2015. Chem. Commun. 51, 11968–11971.

Ahn, M.S., Ahmad, R., Bhat, K.S., Yoo, J.Y., Mahmoudi, T., Hahn, Y.B., 2018. J. Colloid Interface Sci. 518, 277–283.

Amini, A., Varsaneux, O., Kelly, H., Tang, W., Chen, W., Boeras, D.I., Falconer, J., Tucker, J.D., Chou, R., Ishizaki, A., Easterbrook, P., Peeling, R.W., 2017. BMC Infect. Dis. 17.

Aroonyadet, N., Wang, X., Song, Y., Chen, H., Cote, R.J., Thompson, M.E., Datar, R.H., Zhou,

C., 2015. Nano Lett. 15, 1943–1951.

Aydoğdu, G., Zeybek, D.K., Pekyardımcı, Ş., Kılıç, E., 2013. Artif. Cells, Nanomedicine, Biotechnol. 41, 332–338.

Basu, J., Baral, A., Samanta, N., Mukherjee, N., Roychaudhuri, C., 2018. J Electrochem Soc. 165.

Basu, J., Chaudhuri, C.R., 2016. IEEE Electron Device Lett. 37, 492–495.

Bonino, F., Piratvisuth, T., Brunetto, M.R., Liaw, Y.-F., 2010. Antivir. Ther. 15, 35–44.

Cerino, A., Bremer, C.M., Glebe, D., Mondelli, M.U., 2015. Plos One 10.

Chakraborty, W., Ray, R., Samanta, N., RoyChaudhuri, C., 2017. Biosens. Bioelectron. 98, 180–188.

Chen, Y.C., De Oteyza, D.G., Pedramrazi, Z., Chen, C., Fischer, F.R., Crommie, M.F., 2013. ACS Nano 7, 6123–6128.

Choi, Y.H., Lee, G.Y., Ko, H., Chang, Y.W., Kang, M.J., Pyun, J.C., 2014. Biosens. Bioelectron. 56, 286–294.

Chu, C.H., Sarangadharan, I., Regmi, A., Chen, Y.W., Hsu, C.P., Chang, W.H., Lee, G.Y., Chyi, J.I., Chen, C.C., Shiesh, S.C., Lee, G. Bin, Wang, Y.L., 2017. Sci. Rep. 7, 1–15.

Corso, C.D., Dickherber, A., Hunt, W.D., 2008. Biosens. Bioelectron. 24, 805–811.

Dang, V.Q., Trung, T.Q., Duy, L.T., Kim, B.Y., Siddiqui, S., Lee, W., Lee, N.E., 2015. ACS Appl. Mater. Interfaces 7, 11032–11040.

Das, N., RoyChaudhuri, C., 2015. IEEE Trans. Device Mater. Reliab. 15, 402–409.

Das, R.D., Maji, S., Das, S., RoyChaudhuri, C., 2010. Appl. Surf. Sci. 256, 5867–5875.

Diware, M.S., Cho, H.M., Chegal, W., Cho, Y.J., O, S.W., Paek, S.-H., Kim, D.S., Kim, K.-S., Min, Y.G., Jo, J.H., Shin, C., 2017. Biointerphases 12.

Eksin, E., Erdem, A., 2016. Electroanalysis 28, 2514–2521.

Fathollahzadeh, M., Hosseini, M., Norouzi, M., Ebrahimi, A., Fathipour, M., Kolahdouz, M., Haghighi, B., 2017. J. Solid State Electrochem. 22, 61–67.

Gao, N., Gao, T., Yang, X., Dai, X., Zhou, W., Zhang, A., Lieber, C.M., 2016. Proc. Natl. Acad. Sci. 113, 14633–14638.

Gao, N., Zhou, W., Jiang, X., Hong, G., Fu, T.M., Lieber, C.M., 2015. Nano Lett. 15, 2143–2148.

Ghosh, H., Roychaudhuri, C., 2013. Appl. Phys. Lett. 102.

Gilbert, R.J.C., Beales, L., Blond, D., Simon, M.N., Lin, B.Y., Chisari, F. V, Stuart, D.I., Rowlands, D.J., 2005. Proc. Natl. Acad. Sci. U. S. A. 102, 14783–14788.

Hakimian, F., Ghourchian, H., Hashemi, A.S., Arastoo, M.R., Behnam Rad, M., 2018. Sci. Rep. 8, 1–9.

Han, J.H., Lee, D., Chew, C.H.C., Kim, T., Pak, J.J., 2016. Sensors Actuators, B Chem. 228, 36–42.

Hidaka, H., Nowaki, K., Muguruma, H., 2016. iopSCIENCE 01, 1–6.

Ibupoto, Z.H., Ali, S.M.U., Khun, K., Chey, C.O., Nur, O., Willander, M., 2011. Biosensors 1, 153–163.

Kulkarni, G.S., Zhong, Z., 2012. Nano Lett. 12, 719–723.

Kumar, N., Senapati, S., Kumar, S., Kumar, J., Panda, S., 2016. J. Phys. Conf. Ser. 704.

Lee, J., Jang, J., Choi, B., Yoon, J., Kim, J.Y., Choi, Y.K., Myong Kim, D., Hwan Kim, D., Choi, S.J., 2015. Sci. Rep. 5, 1–6.

Lee, S., Cho, J., Lee, Y., Jeon, S., Cha, H.J., Moon, W., 2012. Measurement of hepatitis B surface antigen concentrations using a piezoelectric microcantilever as a mass sensor. J. Sensors 2012, 1-6.

Lei, Y.M., Xiao, M.M., Li, Y.T., Xu, L., Zhang, H., Zhang, Z.Y., Zhang, G.J., 2017. Biosens. Bioelectron. 91, 1–7.

Li, G., Xie, D., Feng, T., Xu, J., Zhang, X., Ren, T., 2014. Solid. State. Electron. 95, 32–35.

Li, X., Zhao, C., Liu, X., 2015. Microsystems Nanoeng. 1, 15014.

Liu, W.-R., Lin, B.-H., Lin, C.-Y., Yang, S., Kuo, C.-C., Chien, F.S.-S., Chang, C.-S., Hsu, C.-H., Hsieh, W.-F., 2015. RSC Advances 5, 12358–12364.

Marques, I., Pinto da Costa, J., Justino, C., Santos, P., Duarte, K., Freitas, A., Cardoso, S., Duarte, A., Rocha-Santos, T., 2017. Int. J. Environ. Anal. Chem. 97, 597–605.

Nam, H., Oh, B.R., Chen, P., Yoon, J.S., Wi, S., Chen, M., Kurabayashi, K., Liang, X., 2015. Appl. Phys. Lett. 107.

Paul, S., Das, A., Chakraborty, A., Chakraborty, B., Palit, M., Chattopadhyay, D., Chattopadhyay, S., 2014. 1st Int. Sci. Technol. Congr. 467–471.

Rutstein, S.E., Kamwendo, D., Lugali, L., Thengolose, I., Tegha, G., Fiscus, S.A., Nelson, J.A.E., Hosseinipour, M.C., Sarr, A., Gupta, S., Chimbwandira, F., Mwenda, R., Mataya, R., 2014. J. Clin. Virol. 60, 392–398.

Shakoori, Z., Salimian, S., Kharrazi, S., Adabi, M., Saber, R., 2014. Anal. Bioanal. Chem. 407, 455–461.

Shariati, M., 2018. Biosens. Bioelectron. 105, 58–64.

Trépo, C., Zoulim, F., Alonso, C., Petit, M.-A., Pichoud, C., Vitvitski, L., 1993. Gut 34, 20–25.

Wang, C., Cui, X., Li, Y., Li, H., Huang, L., Bi, J., Luo, J., Ma, L.Q., Zhou, W., Cao, Y., Wang, B., Miao, F., 2016. Sci. Rep. 6, 1–8. Xiang, Q., Huang, J., Huang, H., Mao, W., Ye, Z., 2018. RSC Adv. 8, 1820–1825.

Xue, C., Kung, C.C., Gao, M., Liu, C.C., Dai, L., Urbas, A., Li, Q., 2015. Sens. Bio-Sensing Res. 3, 7–11.

Yu, X., Xia, Y., Tang, Y., Zhang, W.L., Yeh, Y.T., Lu, H., Zheng, S.Y., 2017. Small 13, 1–12.

Zong, X., Zhang, Z., Zhu, R., 2017. Ieee Sensors 1–3.

Figure Captions:

Figure 1(a). Schematic illustration of the FET Sensor with lateral electrode configuration

Figure 1(b). Schematic illustration of the FET Sensor with vertical electrode configuration

Figure 1(c). Overall picture of FET sensor

Figure 2(a). FESEM image of ZnO seed layer

Figure 2(b). FESEM image of ZnO nanorods (top view)

Figure 2(c). FESEM image of ZnO nanorods (side view)

Figure 2(d). FESEM image of sensor surface after antibody attachment

Figure 3(a). Variation of I_d with V_{gs} before and after antibody attachment condition at different frequencies for lateral electrode configuration

Figure 3(b). Variation of I_d with V_{gs} before and after antibody attachment condition at different frequencies for vertical electrode configuration

Figure 3(c). and Figure 3(d). Electric field line distribution for lateral electrode configuration

Figure 3(e). Electric field line distribution for vertical electrode configuration

Highlights

- Detection of Hepatitis-B surface antigen at the attomolar level in serum using antibody functionalized liquid gated ZnO nanorods field effect transistor (FET) biosensor with vertical electrode configuration.
- Enhanced penetration of the electric field lines through the nanorods improves the limit of detection and sensitivity compared to that of the conventional lateral electrode configuration

- Combined effect of the probable change in the threshold voltage and the carrier mobility for vertical electrode configuration has lead to a sensitivity of around 66% at 1 fM (which is an enhancement by 200%) and a detection limit of 20 aM with a dynamic range from 20 aM to 1 pM.